JACS
JOURNAL OF THE AMERICAN CHEMICAL SOCIETY
Article
pubs.acs.org/JACS

Mechanism and Origins of Ligand-Controlled Selectivities in [Ni(NHC)]-Catalyzed Intramolecular (5 + 2) Cycloadditions and Homo-Ene Reactions: A Theoretical Study

Xin Hong, Peng Liu, and K. N. Houk*

Department of Chemistry and Biochemistry, University of California, Los Angeles, California 90095-1569, United States

Supporting Information

ABSTRACT: The mechanism and origins of selectivities in [Ni(NHC)]-catalyzed intramolecular (5 + 2) cycloadditions and homo-ene reactions of vinylcyclopropanes (VCPs) and alkynes have been studied using density functional theory. The preferred mechanism involves oxidative alkyne−alkene cyclization to form a metallacyclopentene intermediate, in contrast to a cyclopropane cleavage pathway in the reaction with Rh(I) catalysts. The selectivity between the (5 + 2) and homo-ene products is determined in the subsequent competing reductive elimination and β-hydride elimination steps. Two similar-sized N-heterocyclic carbene (NHC) ligands, SIPr and I*t*Bu, yielded reversed product selectivity, favoring the (5 + 2) and homo-ene products respectively. This is attributed to the anisotropic steric environment of these NHC ligands, which positions the bulky substituents on the ligand toward different directions and leads to distinct steric control in the reductive elimination and β-hydride elimination transition states.

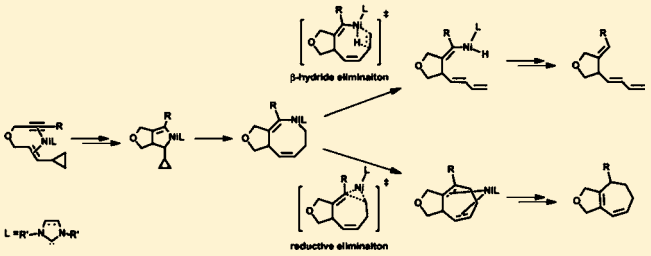

INTRODUCTION

As the structural core in a large number of biologically important natural products, functionalized seven-membered rings are targets for numerous synthetic studies. Among the current methodologies, transition-metal-catalyzed (5 + 2) cycloadditions of vinylcyclopropanes (VCPs) with 2π components such as alkynes, alkenes, and allenes provide a step-economical methodology for the synthesis of functionalized cycloheptadienes.[1] Since the first report using a Rh(I) catalyst by Wender et al.,[2] various transition metal catalysts including rhodium,[3] ruthenium,[4] nickel,[5] and iron[6] have shown promising catalytic activities in this methodology. The (5 + 2) reaction also led to the discovery of (5 + 1), (5 + 2 + 1), and other cycloadditions employing vinylcyclopropane or its analogues as building blocks.[7]

In contrast to the vast aspects of experimental investigations on this reaction, computational studies have only been focused on Rh-catalyzed reactions to date.[8] The effects of metal catalysts on the mechanism and selectivity are still not clear. Especially, although all (5 + 2) cycloadditions are likely to occur via a metallacyclooctadiene intermediate (**7**, Scheme 1), the mechanism leading to the formation of this intermediate may be different when different metal catalysts are employed. Previous computational studies indicated that the cycloadditions with Rh catalysts occur via cleavage of the cyclopropane to form the metallacyclohexene intermediate **5** followed by alkyne insertion to form intermediate **7** (Step A, Scheme 1). The alternative mechanism involving oxidative cyclization of the alkyne and the alkenyl group on a VCP to form the metallacyclopentene intermediate **6** (Step B) is not favorable with Rh. Since vinylcyclopropane is a widely used synthon, its behavior as a 2C or 5C component at the initial step with different transition metal catalysts not only directly relates to the mechanism in the (5 + 2) cycloadditions but also impacts the synthetic utility of VCPs in other transition-metal-catalyzed reactions.

Scheme 1. Postulated Mechanisms for Transition-Metal-Catalyzed (5 + 2) Cycloadditions

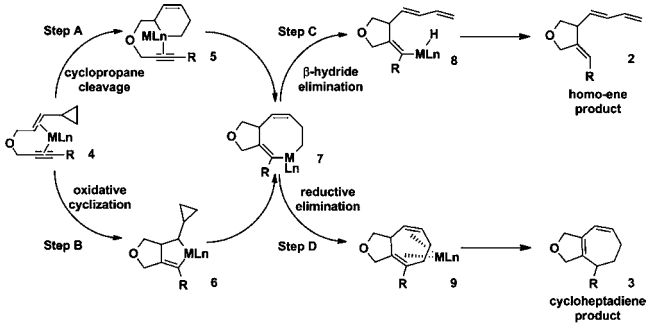

In addition to the uncertainty of the initial steps in the mechanism, the metal catalysts may also affect the mechanism in the subsequent steps after formation of the metallacyclooctadiene intermediate. Unique among all metal catalysts for (5 + 2) cycloadditions, nickel shows strong ligand control in the selectivity of the (5 + 2) cycloaddition product (**3**) and a homo-ene product (**2**).[9] Using the SIPr (1,3-bis(2,6-diisopropylphenyl)-imidazolidene) ligand, the selectivity between the cycloheptadiene

Received: October 5, 2012
Published: December 31, 2012

dx.doi.org/10.1021/ja309873z | J. Am. Chem. Soc. 2013, 135, 1456−1462

Scheme 2. Nickel-NHC Catalyzed Intramolecular (5 + 2) Cycloaddition and Homo-Ene Reaction of Alkyne and VCP

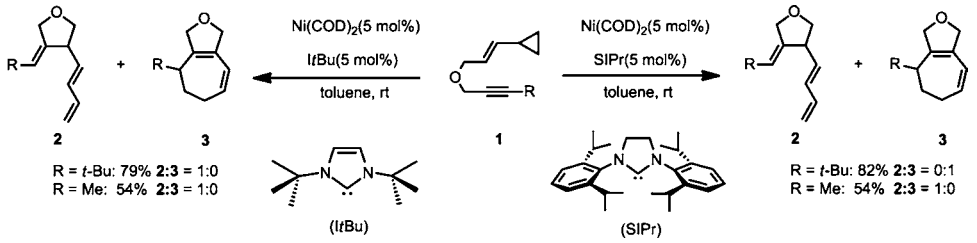

product **3** and homo-ene product **2** depends upon the nature of the terminal alkyne substituent. In contrast, the reaction with the I*t*Bu ligand gives only the homo-ene product **2** regardless of the terminal alkyne substituent (Scheme 2). In addition, the tether between the VCP and 2π component has no significant effect on the selectivity.[10]

Apparently, the selectivity between the cycloheptadiene and the homo-ene products is controlled by the preference for the β-hydride elimination and the reductive elimination pathways after the formation of the metallacyclooctadiene intermediate. Controlling the competition between reductive elimination and β-hydride elimination to prevent side reactions[11] and catalyst decomposition[12] is a persistent challenge in many transition-metal-catalyzed C−C bond formation reactions. In order to achieve better synthetic utility, great efforts have been made to control these competitive steps by optimization of the substrate,[13] the counterion,[14] and especially the type and size of the ligand.[15] Since SIPr and I*t*Bu are both electron-rich NHC ligands, their steric properties are most likely controlling the selectivity. Based on the widely applied "buried volume" (%V_{bur}) model,[16] which describes the average bulkiness of the ligand, I*t*Bu (35.5%V_{bur})[16e] and SIPr (35.7%V_{bur})[16e] have almost identical steric bulk. Why do these two NHC ligands with similar steric and electronic properties lead to reversed selectivity between β-hydride elimination and reductive elimination? Here we report DFT calculations on the transition states of the competing pathways and analyze the effects of the shape of NHC ligands, i.e. the orientation of the bulky substituents, with the steric contour model. We[17] and Cavallo[18] have employed the steric contour model to highlight the importance of the anisotropic steric environment of NHC ligands in determining regio- and stereoselectivities. In this report, we present the first example that the shape and orientation of the NHC ligand affect the mechanism and prevent β-hydride elimination from the metallacycle.

COMPUTATIONAL DETAILS

Geometry optimizations, frequencies, and solvation energy calculations were performed with the B3LYP functional implemented in Gaussian 09.[19] The Stuttgart/Dresden effective core potential (SDD) was used for nickel. For all other atoms, the 6-31G(d) basis set was employed in geometry optimizations and the 6-311+G(2d,p) basis set was employed in single-point solvation energy calculations. All reported free energies involve zero-point vibrational energy corrections, thermal corrections to the Gibbs free energy at 298 K, DFT-D3 dispersion corrections,[20] and solvation free energy corrections computed by single-point CPCM calculations on gas-phase optimized geometries. Toluene was used in the CPCM calculations for consistency with experiment. The molecular cavities were built up using the United Atom Topological Model (UAHF), and an extra sphere was added on the transferred hydrogen of **TS25** and **TS29**. Figures 2, 4, 6, and 7 were prepared using CYLView.[21]

RESULTS AND DISCUSSION

1. Mechanism of Formation of the Metallacyclooctadiene Intermediate. The possible pathways of the transformation of the substrate coordinated complex **10** to the metallacyclooctadiene intermediate **14** are computed and summarized in Figure 1. The structures of selected intermediates

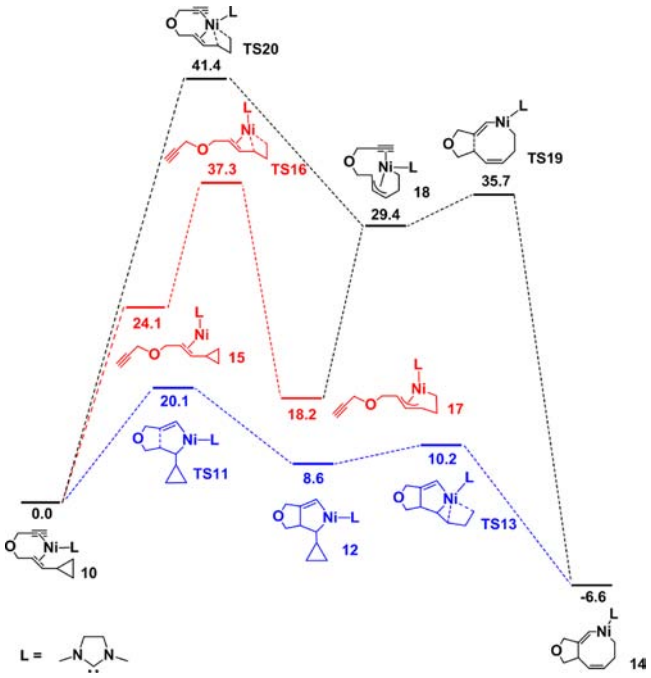

Figure 1. Gibbs free energies for [Ni(NHC)]-catalyzed cycloaddition from substrate coordinated complex to metallacyclooctadiene intermediate. The favored oxidative cyclization pathway is shown in blue, while the black and red indicate the cyclopropane cleavage pathway with alkyne coordination before (black) or after (red) VCP cleavage. Energies are given in kcal/mol.[22]

and transition states are shown in Figure 2. A model NHC ligand, 1,3-dimethylimidazolidine, was employed in the investigation of mechanisms.

To form the metallacyclooctadiene intermediate, formation of one C−C bond and two Ni−C bonds are the fundamental steps, and the order of these steps determines whether the oxidative cyclization mechanism via the metallacyclopentene intermediate **12** or the cyclopropane cleavage mechanism via the metallacyclohexene intermediate **18** is involved.[23] In the oxidative cyclization mechanism (highlighted in blue in Figure 1), complex **10** initially undergoes C−C bond formation via transition state **TS11** (20.1 kcal/mol) to give the metallacyclopentene intermediate **12** (8.6 kcal/mol). Subsequent cleavage of the cyclopropane is more facile with a 1.6 kcal/mol barrier to give the stable metallacyclooctadiene intermediate **14** (−6.6 kcal/mol). On the

dx.doi.org/10.1021/ja309873z | J. Am. Chem. Soc. 2013, 135, 1456−1462

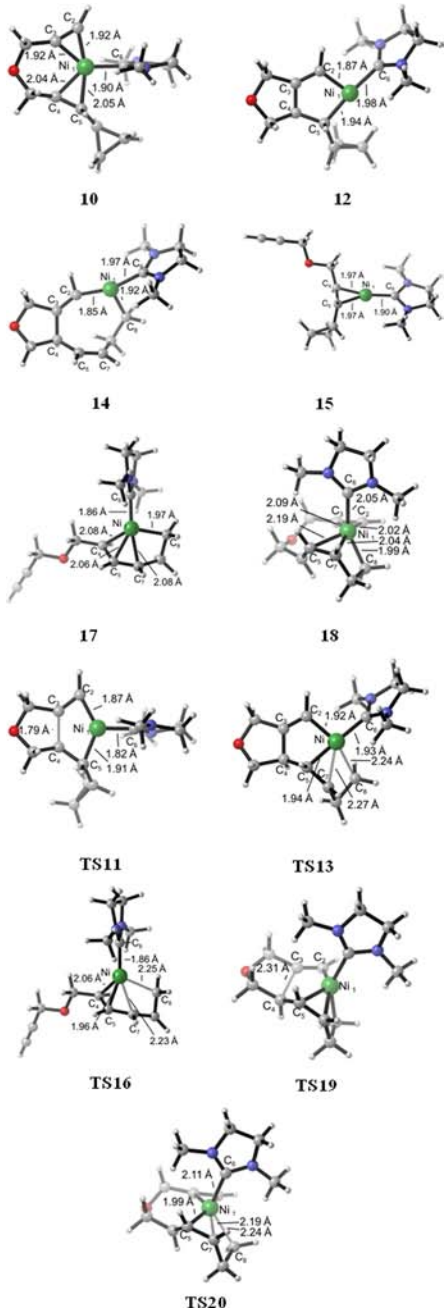

Figure 2. Optimized structures and bond distances of selected intermediates and transition states in Figure 1.

other hand, initial cleavage of the cyclopropane to give the metallacyclohexene intermediate **18** (29.4 kcal/mol) is very different. The cyclopropane cleavage can occur in two ways.[24] Figure 1 shows that whether the alkyne is coordinated to the metal in the TS or not (**TS20** and **TS16**, respectively), the reaction requires a much higher barrier than the oxidative cyclization (**TS11**). Although [Ni(NHC)] can promote the rearrangement of vinylcyclopropane to cyclopentene via cyclopropane cleavage,[24] it is not likely to occur in this reaction. The main reason is the strong intramolecular coordination with alkyne. The dissociation of alkyne from the catalyst resting state **10** requires 24.1 kcal/mol. This contributes to the high barrier of cyclopropane cleavage transition state **TS16**. The cyclopropane cleavage transition state involves coordination of the alkyne (**TS20**), requiring an even higher activation energy than **TS16**. This is attributed to the formation of an unstable intermediate (**18**) in this pathway. Thus the most preferred pathway in [Ni(NHC)] catalyzed (5 + 2) cycloadditions initiates via oxidative alkyne−alkene cyclization to form the metallacyclopentene intermediate **12**.[25] This is contrast to the Rh(I) catalyst from our previous theoretical studies.[8] In $[Rh(CO)_2Cl]_2$ catalyzed intermolecular (5 + 2) cycloadditions of VCP and acetylene, the cyclopropane cleavage pathway is preferred by 7.8 kcal/mol.[8a] This reversed preference arises from two parts. First, the electron-rich NHC ligand stabilizes the 14-electron oxidative coupling transition state **TS11** dramatically with only a 20.1 kcal/mol barrier. In $[Rh(CO)_2Cl]_2$, this step requires a barrier of 29.7 kcal/mol in the intermolecular reaction. Also, the relative stability between intermediates **10** and **15** are very different between nickel and rhodium complexes. From the triangular geometry of **15**, the rotation of cyclopropane will not provide any favorable agostic interaction to replace alkyne coordination as in the rhodium complex. Therefore, rhodium and nickel have different preferences between metallacyclohexene and metallacyclopentene pathways.

2. Mechanism of the Formation of (5 + 2) Cycloaddition and Homo-Ene Products. From the metallacyclooctadiene intermediate **14** (−6.6 kcal/mol with respect to the reactant complex **10**), there are two different pathways. First, direct C−C reductive elimination could occur via transition state **TS21** (7.9 kcal/mol), leading to the cycloheptadiene product **22** (−26.5 kcal/mol) (Figures 3 and 4). Then diene isomerization

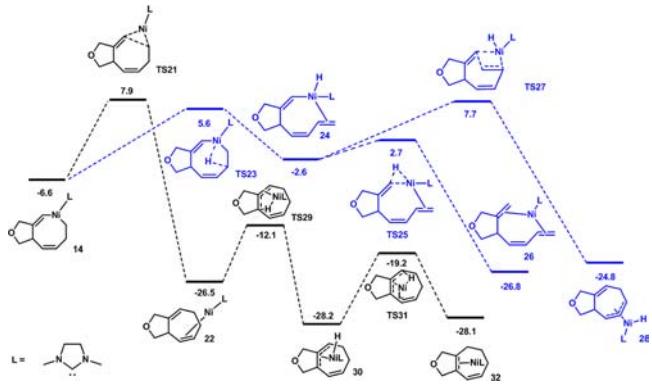

Figure 3. Gibbs free energies of the [Ni(NHC)]-catalyzed (5 + 2) cycloaddition and homo-ene reaction from the metallacyclooctadiene intermediate **14**. The (5 + 2) cycloaddition pathway is shown in black, and the homo-ene pathway is shown in blue. Energies are given in kcal/mol.

occurs via transition state **TS29** (−12.1 kcal/mol), generating an allyl nickel(II) hydride intermediate **30** (−28.2 kcal/mol). From **30**, reductive elimination occurs via **TS31** (−19.2 kcal/mol), leading to a more stable conjugated diene product complex **32** (−28.1 kcal/mol). The overall barrier for cycloheptadiene generation is only 14.5 kcal/mol (**14** to **TS21**). Alternatively, *β*-hydride transfer could occur through **TS23** (5.6 kcal/mol), forming a tetracoordinated nickel(II) hydride complex **24** (−2.6 kcal/mol). This relatively unstable intermediate undergoes C−H reductive elimination to form the triene product **26** (−26.8 kcal/mol) via transition state **TS25** (2.7 kcal/mol). A possible alkene insertion transition state **TS27** (7.7 kcal/mol) from **24** was also located, generating a nickel hydride complex **28**. In principle, **28** can further undergo C−H reductive elimination and generate the intermediate **22** and eventually the seven-membered ring product. Therefore, **TS21** and **TS27** are very competitive with the model ligand and further calculations with

dx.doi.org/10.1021/ja309873z | J. Am. Chem. Soc. 2013, 135, 1456−1462

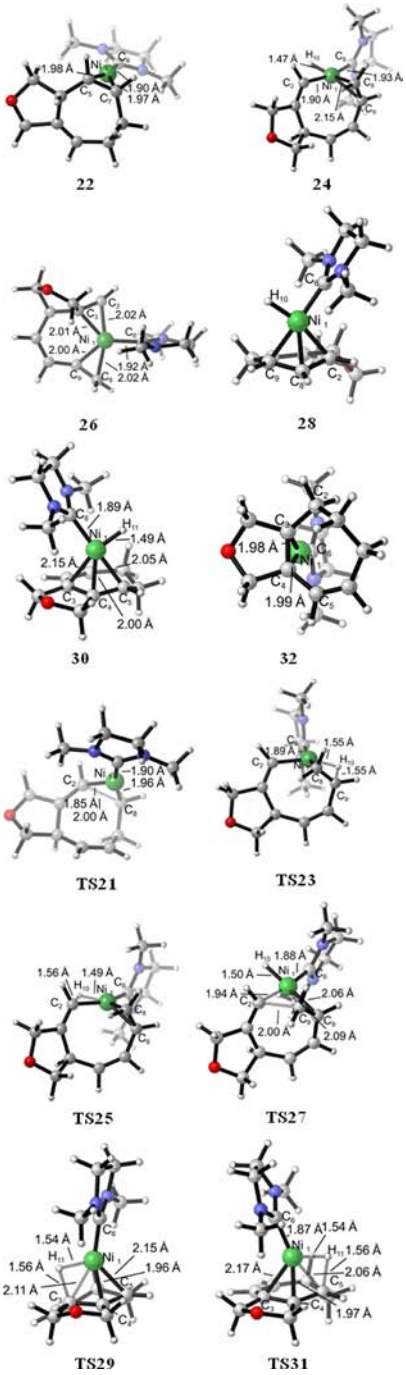

Figure 4. Optimized structures and bond distances of selected intermediates and transition states in Figure 3.

the experimental ligand SIPr were conducted to determine the favored pathway for cycloheptadiene formation. **TS21-SIPr** is 4.6 kcal/mol more stable than **TS27-SIPr**, suggesting that C−C reductive elimination and β-hydride elimination pathways (**TS21** and **TS23**) are the selectivity-determining steps for (5 + 2) cycloaddition and homo-ene reaction.

3. The Catalytic Cycle. The full catalytic cycles for [Ni(NHC)]-catalyzed (5 + 2) cycloaddition and homo-ene reaction are shown in Figure 5. The substrate coordinated nickel complex **10** is the resting state in both catalytic cycles. Complex **10** undergoes alkyne−alkene cyclization to form a metallacyclopentene intermediate **12**. Subsequent cyclopropane cleavage of **12** leads to metallacyclooctadiene intermediate **14**. From intermediate **14**, the reductive elimination produces the cycloheptadiene complex **22** or β-hydride elimination occurs through transition state **TS23** to eventually give triene complex **26**. The isomerization from **22** is facile and further produces the observed cycloheptadiene coordinated complex **32**. The liberation of the product from both product complexes **32** and **26** to regenerate the Ni-reactant complex **10** is highly exothermic. The predicted barrier of 20.1 kcal/mol is consistent with experimental conditions.[26]

4. Substituent and Ligand Effects on Selectivities between (5 + 2) and Homo-Ene Products. *4.1. SIPr Controlled Selectivity.* When the SIPr ligand is employed, the preference for the formation of **2** or **3** relies on the terminal alkyne substituent in the substrate (Table 1).[5] When the alkyne substituent is small, e.g. methyl or ethyl, the major product is triene **2**. With a bulky substituent, such as isopropyl or tertiary-butyl, cycloheptadiene **3** is formed. The catalytic cycles (shown in Figure 5) indicated the selectivity of the triene (**2**) and cycloaddition (**3**) products is determined by the energy difference between **TS23** and **TS21**. The transition states in reactions with the SIPr ligand and substrates with various alkyne substituents were computed.

Table 1 shows the computational and experimental selectivities between **2** and **3**. Computations predicted the same trend of selectivity as the experiment. In the reactions with the SIPr ligand, bulkier alkyne substituents (e.g., R = *t*-Bu or TMS, entries 4 and 5) prefer the cycloaddition product **3**, while in the reaction with the I*t*Bu ligand, the triene product **2** is favored (entry 6). In cases where moderate selectivities were observed experimentally (entries 2 and 3), computation showed a greater preference for **3** than experiment.

Figure 6 shows the transition states in the reactions with Me and TMS substituted substrates and the SIPr ligand. For each reaction, both the reductive elimination transition state (**TS21**) leading to the (5 + 2) cycloaddition product and the β-hydride elimination transition state (**TS23**) leading to the homo-ene product are shown. The conformations of the metallacycle in **TS21** and **TS23** are similar, while the orientations of the SIPr ligand are noticeably different. In the reductive elimination transition state (**TS21**), the imidazolidine ring is in the same plane with the Ni and the forming carbon−carbon bond. In contrast, in the β-hydride elimination transition state (**TS23**), the imidazolidine ring is perpendicular to the plane of Ni and the two α-carbon atoms. To illustrate the different orientations of the NHC ligands, 2D contour maps of the van der Waals surface of the SIPr ligand in transition states **TS21** and **TS23** are generated and shown in Figure 6. The red region in the contour plot indicates the ligand is closer to the substrate, and the blue region indicates the ligand is farther away from the substrate. The "R" marks the α-positions of the terminal alkyne substituent. In the β-hydride elimination transition state (**TS23**), the alkyne substituent (R) is placed adjacent to two *i*-Pr groups. In contrast, in the reductive elimination transition state (**TS21**), the alkyne substituent (R) is placed under the phenyl rings and the distances between R and *i*-Pr groups are greater than those in **TS23**. In reactions with bulky alkyne substituents, the β-hydride elimination transition state is disfavored due to steric repulsions with the *i*-Pr groups on the ligand. For example, in **TS23-SIPr-TMS** (R = TMS), the shortest H−H distance between TMS and *i*-Pr groups is only 2.10 Å. In **TS21-SIPr-TMS**, the distance between TMS and *i*-Pr become longer, with the shortest H−H distance being 2.28 Å. Thus, β-hydride elimination (**TS23-SIPr-TMS**) is disfavored by 6.1 kcal/mol.

dx.doi.org/10.1021/ja309873z | *J. Am. Chem. Soc.* 2013, 135, 1456−1462

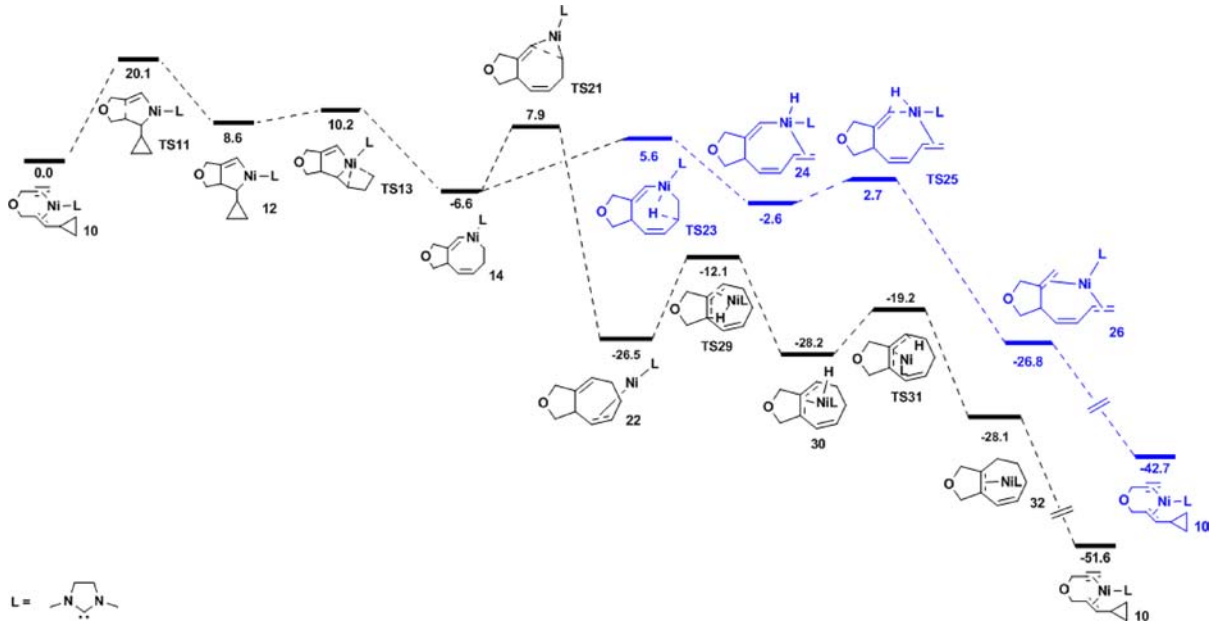

Figure 5. Gibbs free energies of preferred mechanism for [Ni(NHC)]-catalyzed (5 + 2) cycloaddition (black) and homo-ene reaction (blue). Energies are Gibbs free energies given in kcal/mol.

Table 1. Theoretical and Experimental Selectivities between Triene 2 and Cycloheptadiene 3 with SIPr and I*t*Bu Ligands and Substrates with Various Terminal Substituents[a] (Energies are in kcal/mol)

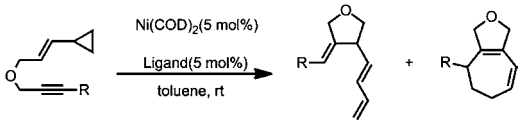

entry	R	ligand	$\Delta\Delta G^{\ddagger}(2-3)^{b}$	2:3^{theo}	2:3^{exp}
1[c]	Me	SIPr	−0.8	85:15	100:0
2	Et	SIPr	2.0	5:95	60:40
3	*i*-Pr	SIPr	2.6	1:99	33:67
4	*t*-Bu	SIPr	3.5	0:100	0:100
5	TMS	SIPr	6.1	0:100	0:100
6	*t*-Bu	I*t*Bu	−1.2	90:10	100:0

[a]The M06 method also produces the same trend with a small preference for (5 + 2) cycloadditions. Detailed results are listed in the Supporting Information. [b]The selectivity between pathways leading to products **2** and **3** is calculated from the activation free energy difference between **TS23** and **TS21**. [c]Replacing the oxygen by NTs in the tether changed the $\Delta\Delta G^{\ddagger}(2-3)$ to 0.2 kcal/mol. Detailed results are listed in the Supporting Information.

When the alkyne substituent is small (e.g., R = Me), the steric effects are diminished and β-hydride elimination becomes favorable over reductive elimination.[27]

*4.2. Selectivity in Reactions with the I*t*Bu Ligand.* The buried volume of the I*t*Bu ligand (35.5%) is almost identical to that of SIPr (35.7%). This suggests the overall bulkiness of these ligands is similar. However, the reaction with the I*t*Bu ligand gives reversed selectivity compared to the SIPr ligand (entries 6 and 4, Table 1). The β-hydride elimination transition state **TS23-I*t*Bu-*t*Bu** is favored by 1.2 kcal/mol, leading to the homo-ene product, while, in the reaction with SIPr ligand, β-hydride elimination is disfavored by 3.5 kcal/mol. The optimized transition structures of reductive elimination and β-hydride elimination with the I*t*Bu

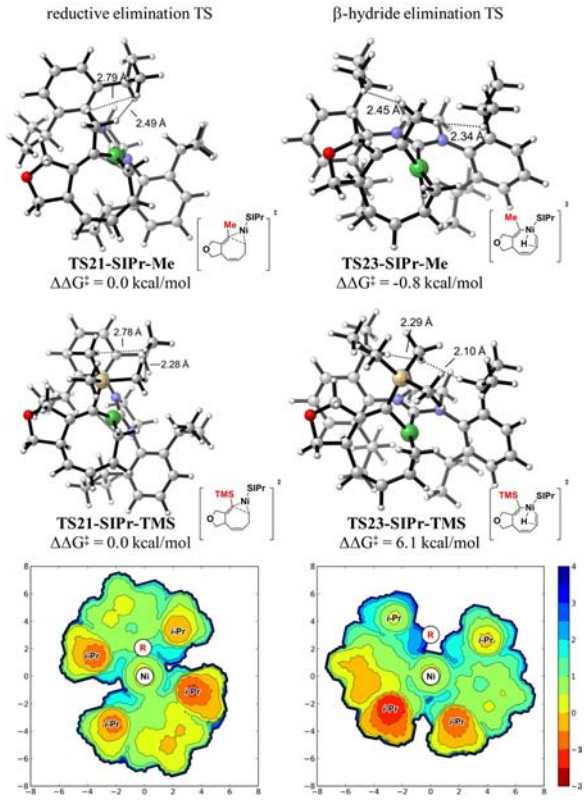

Figure 6. Optimized transition structures of Me and TMS substituted **TS21** (reductive elimination in the (5 + 2) pathway) and **TS23** (β-hydride elimination in the homo-ene pathway) with the SIPr ligand. Steric contour plots of the SIPr ligand are shown for both TSs and illustrate the different orientations of the NHC ligand in **TS21** and **TS23**. Ni is located at the origin of the coordinate system in the contour plots. The contour line of zero is defined as in the same plane with the Ni atom. Negative distance (red) indicates the ligand is closer to the substrate; positive distance (blue) indicates the ligand is farther away from the substrate. Distances are in Å.

dx.doi.org/10.1021/ja309873z | *J. Am. Chem. Soc.* 2013, 135, 1456−1462

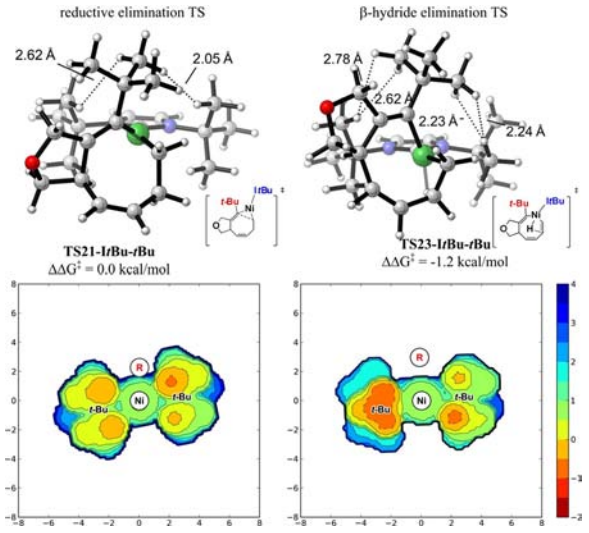

Figure 7. Optimized transition structures of *t*-Bu substituted **TS21** (reductive elimination in the (5 + 2) pathway) and **TS23** (*β*-hydride elimination in the homo-ene pathway) with the I*t*Bu ligand. Steric contour plots of the I*t*Bu ligand are shown for both TSs and illustrate the orientations of the NHC ligand in **TS21** and **TS23**. Ni is located at the origin of the coordinate system in the contour plots. The contour line of zero is defined as in the same plane with the Ni atom. Negative distance (red) indicates the ligand is closer to the substrate; positive distance (blue) indicates the ligand is farther away from the substrate. Distances are in Å.

ligand are shown in Figure 7. Ligand steric contour plots for these transition states are also illustrated. The ligand contour plots indicated the shape of the I*t*Bu ligand is very different from that of the SIPr ligand, although their buried volume and overall bulkiness are similar. The most bulky regions on the I*t*Bu ligand are the two *t*-Bu groups located in the same plane with the imidazolylidene ring. In the *β*-hydride elimination transition state (**TS23-I*t*Bu-*t*Bu**), the orientation of the I*t*Bu ligand is the same as that of the SIPr ligand (**TS23-SIPr-Me** and **TS23-SIPr-TMS**, Figure 6) and the smaller model ligand SIMe (**TS23**, Figure 4): the alkyne substituent (marked with a red "R" in the contour plot) is placed perpendicular to the imidazolylidene ring, and thus no obvious steric repulsions with the ligand are observed. In the reductive elimination transition state (**TS21-I*t*Bu-*t*Bu**), the I*t*Bu ligand adopts a different orientation from those in the reductive elimination with the SIPr and SIMe ligands (**TS21-SIPr-Me** and **TS21-SIPr-TMS**, Figure 6 and **TS21**, Figure 4). Steric repulsions with the *t*-Bu groups in the imidazolylidene plane forced the I*t*Bu ligand to rotate almost 90° to place the alkyne substituent perpendicular to the imidazolylidene. The distance between the alkyne substituent and the *t*-Bu groups on the ligand is shorter in the reductive elimination TS than that in the *β*-hydride elimination TS.

CONCLUSION

The mechanism and selectivities of [Ni(NHC)]-catalyzed (5 + 2) cycloadditions and homo-ene reactions were studied theoretically. The origins of the selectivity of the cycloaddition and homo-ene products in reactions with different alkyne substituents and ligands were elucidated. The preferred catalytic cycle involves oxidative cyclization to form a metallacyclopentene intermediate, followed by cyclopropane cleavage to yield a metallacycloctadiene intermediate. Subsequent direct C−C reductive elimination leads to the cycloheptadiene product, while *β*-hydride elimination and C−H reductive elimination lead to the homo-ene product. The selectivity is controlled by the shape and orientation of the NHC ligand. With the SIPr ligand, larger terminal alkyne substituents destabilize the *β*-hydride elimination transition state, leading to the (5 + 2) cycloaddition product. This is attributed to the steric repulsions with the *i*-Pr groups located perpendicular to the imidazolidine ring. With the I*t*Bu ligand, the *β*-hydride elimination transition state leading to the homo-ene product is preferred.

ASSOCIATED CONTENT

Supporting Information

Optimized Cartesian coordinates and energies, M06-calculated results of ligand-controlled selectivities, and complete ref 19 (Gaussian 09). This material is available free of charge via the Internet at http://pubs.acs.org.

AUTHOR INFORMATION

Corresponding Author

houk@chem.ucla.edu

Notes

The authors declare no competing financial interest.

ACKNOWLEDGMENTS

We are grateful to the National Science Foundation (CHE-0548209) for financial support of this research. We thank Professors Paul A. Wender and Janis Louie and Dr. Yu Lan for helpful discussions. Calculations were performed on the Hoffman2 cluster at UCLA and the Extreme Science and Engineering Discovery Environment (XSEDE), which is supported by the NSF (OCI-1053575).

REFERENCES

(1) For recent reviews of transition-metal-catalyzed (5 + 2) cycloadditions: (a) Wender, P. A.; Gamber, G. G.; Williams, T. J. In *Modern Rhodium-Catalyzed Organic Reactions*; Evans, P. A., Ed.; Wiley-VCH: Weinheim, 2005; pp 263−299. (b) Wender, P. A.; Croatt, M. P.; Deschamps, N. M. In *Comprehensive Organometallic Chemistry III Vol. 10*; Crabtree, R. H., Mingos, D. M. P., Eds.; Elsevier, Oxford, 2007; pp 603−647. (c) Butenschön, H. *Angew. Chem., Int. Ed.* **2008**, *47*, 5287. (d) Pellissier, H. *Adv. Synth. Catal.* **2011**, *353*, 189.

(2) Wender, P. A.; Takahashi, H.; Witulski, B. *J. Am. Chem. Soc.* **1995**, *117*, 4720.

(3) (a) Wender, P. A.; Rieck, H.; Fuji, M. *J. Am. Chem. Soc.* **1998**, *120*, 10976. (b) Wender, P. A.; Sperandio, D. *J. Org. Chem.* **1998**, *63*, 4164. (c) Gilbertson, S. R.; Hoge, G. S. *Tetrahedron Lett.* **1998**, *39*, 2075. (d) Wender, P. A.; Dyckman, A. J.; Husfeld, C. O.; Scanio, M. J. C. *Org. Lett.* **2000**, *2*, 1609. (e) Wang, B.; Cao, P.; Zhang, X. *Tetrahedron Lett.* **2000**, *41*, 8041. (f) Wender, P. A.; Barzilay, C. M.; Dyckman, A. J. *J. Am. Chem. Soc.* **2001**, *123*, 179. (g) Wender, P. A.; Gamber, G. G.; Scanio, M. J. C. *Angew. Chem., Int. Ed.* **2001**, *40*, 3895. (h) Wender, P. A.; Williams, T. J. *Angew. Chem., Int. Ed.* **2002**, *41*, 4550. (i) Wender, P. A.; Love, J. A.; Williams, T. J. *Synlett* **2003**, 1295. (j) Wegner, H. A.; de Meijere, A.; Wender, P. A. *J. Am. Chem. Soc.* **2005**, *127*, 6530. (k) Wender, P. A.; Haustedt, L. O.; Lim, J.; Love, J. A.; Williams, T. J.; Yoon, J.-Y. *J. Am. Chem. Soc.* **2006**, *128*, 6302. (l) Lee, S. I.; Park, Y.; Park, J. H.; Jung, G.; Choi, S. Y.; Chung, Y. K.; Lee, B. Y. *J. Org. Chem.* **2006**, *71*, 91. (m) Saito, A.; Ono, T.; Hanzawa, Y. *J. Org. Chem.* **2006**, *71*, 6437. (n) Gomez, F. J.; Kamber, N. E.; Deschamps, N. M.; Cole, A. P.; Wender, P. A.; Waymouth, R. M. *Organometallics* **2007**, *26*, 4541. (o) Shintani, R.; Nakatsu, H.; Takatsu, K.; Hayashi, T. *Chem.—Eur. J.* **2009**, *15*, 8692. (p) Liu, P.; Sirois, L. E.; Cheong, P. H. Y.; Yu, Z. X.; Hartung, I. V.; Rieck, H.; Wender, P. A.; Houk, K. N. *J. Am. Chem. Soc.* **2010**, *132*, 10127. (q) Wender, P. A.; Stemmler, R. T.; Sirois, L. E. *J. Am. Chem. Soc.* **2010**, *132*, 2532. (r) Wender, P. A.; Sirois, L. E.; Stemmler, R. T.; Williams, T.

J. *Org. Lett.* **2010**, *12*, 1604. (s) Wender, P. A.; Lesser, A. B.; Sirois, L. E. *Org. Synth.* **2011**, *88*, 109.
(4) (a) Trost, B. M.; Toste, F. D.; Shen, H. *J. Am. Chem. Soc.* **2000**, *122*, 2379. (b) Trost, B. M.; Shen, H. C. *Org. Lett.* **2000**, *2*, 2523. (c) Trost, B. M.; Shen, H. C. *Angew. Chem., Int. Ed.* **2001**, *40*, 2313. (d) Trost, B. M.; Toste, F. D. *Angew. Chem., Int. Ed.* **2001**, *40*, 1114. (e) Trost, B. M.; Shen, H. C.; Schulz, T. *Org. Lett.* **2003**, *5*, 4149. (f) Trost, B. M.; Shen, H. C.; Horne, D. B.; Toste, E. D.; Steinmetz, B. G.; Koradin, C. *Chem.—Eur. J.* **2005**, *11*, 2577.
(5) Zuo, G.; Louie, J. *J. Am. Chem. Soc.* **2005**, *127*, 5798.
(6) Fürstner, A.; Majima, K.; Martin, R.; Krause, H.; Kattnig, E.; Goddard, R.; Lehmann, C. W. *J. Am. Chem. Soc.* **2008**, *130*, 1992.
(7) (a) Wender, P. A.; Gamber, G. G.; Hubbard, R. D.; Zhang, L. *J. Am. Chem. Soc.* **2002**, *124*, 2876. (b) Wender, P. A.; Gamber, G. G.; Hubbard, R. D.; Pham, S. M.; Zhang, L. *J. Am. Chem. Soc.* **2005**, *127*, 2836. (c) Wang, Y.; Wang, J.; Su, J.; Huang, F.; Jiao, L.; Liang, Y.; Yang, D.; Zhang, S.; Wender, P. A.; Yu, Z.-X. *J. Am. Chem. Soc.* **2007**, *129*, 10060. (d) Jiao, L.; Ye, S. Y.; Yu, Z.-X. *J. Am. Chem. Soc.* **2008**, *130*, 7178. (e) Huang, F.; Yao, Z.-K.; Wang, Y.; Wang, Y.; Zhang, J.; Yu, Z.-X. *Chem.—Asian J.* **2010**, *5*, 1555. (f) Jiao, L.; Lin, M.; Yu, Z.-X. *Chem. Commun.* **2010**, *46*, 1059. (g) Jiang, G.-J.; Fu, X.-F.; Li, Q.; Yu, Z.-X. *Org. Lett.* **2012**, *14*, 692. (h) Lin, M.; Li, F.; Jiao, L.; Yu, Z.-X. *J. Am. Chem. Soc.* **2011**, *133*, 1690. (i) Lin, M.; Kang, G.-Y.; Guo, Y.-A.; Yu, Z.-X. *J. Am. Chem. Soc.* **2012**, *134*, 398. (j) Liang, Y.; Jiang, X.; Fu, X.-F.; Ye, S.; Wang, T.; Yuan, J.; Wang, Y.; Yu, Z.-X. *Chem.—Asian J.* **2012**, *7*, 593.
(8) (a) Yu, Z.-X.; Wender, P. A.; Houk, K. N. *J. Am. Chem. Soc.* **2004**, *126*, 9154. (b) Yu, Z.-X.; Cheong, P. H.-Y.; Liu, P.; Legault, C. Y.; Wender, P. A.; Houk, K. N. *J. Am. Chem. Soc.* **2008**, *130*, 2378. (c) Liu, P.; Cheong, P. H.-Y.; Yu, Z.-X.; Wender, P. A.; Houk, K. N. *Angew. Chem., Int. Ed.* **2008**, *47*, 3939. (d) Montero-Campillo, M. M.; Cabaleiro-Lago, E. M.; Rodriguez-Otero, J. *J. Phys. Chem. A* **2008**, *112*, 9068. (e) Xu, X.-F.; Liu, P.; Lesser, A.; Sirois, L. E.; Wender, P. A.; Houk, K. N. *J. Am. Chem. Soc.* **2012**, *134*, 11012. (f) See ref 3p.
(9) Other products from different β-hydride eliminations can be formed through rhodium and ruthenium catalysts with various preferences. For rhodium catalyst, see: Wender, P. A.; Husfeld, C. O.; Langkopf, E.; Love, J. A. *J. Am. Chem. Soc.* **1998**, *120*, 1940−1941. For ruthenium catalyst, see ref 4.
(10) The oxygen, carbon, and nitrogen tethers give similar selectivities with the same ligand and terminal alkyne substituent; see ref 5. Similar tether effects have also been found in many other related experimental studies on the transition-metal-catalyzed intramolecular cycloadditions involving VCP and 2π components with Rh and Ru catalysts. Switching the tether only has limited effects on the selectivities; see refs 3k, 4f, 7h, and 7i.
(11) (a) Matas, I.; Campora, J.; Palma, P.; Alvarez, E. *Organometallics* **2009**, *28*, 6515. (b) Lan, Y.; Liu, P.; Newman, S. G.; Lautens, M.; Houk, K. N. *Chem. Sci.* **2012**, *3*, 1987.
(12) (a) Eisch, J. J.; Shi, X.; Owuor, F. A. *Organometallics* **1998**, *17*, 5219. (b) Eisch, J. J.; Owuor, F. A.; Shi, X. *Organometallics* **1999**, *18*, 1583. (c) Eisch, J. J.; Adeosun, A. A.; Dutta, S.; Fregene, P. O. *Eur. J. Org. Chem.* **2005**, 2657. (d) Hong, S. H.; Day, M. W.; Grubbs, R. H. *J. Am. Chem. Soc.* **2004**, *126*, 7414. (e) Rensburg, W. J.; Steynberg, P. J.; Meyerm, W. H.; Kirk, M. M.; Forman, G. S. *J. Am. Chem. Soc.* **2004**, *126*, 14332. (f) Hong, S. H.; Wenzel, A. G.; Salguero, T. T.; Day, M. W.; Grubbs, R. H. *J. Am. Chem. Soc.* **2007**, *129*, 7961. (g) Herbert, M. B.; Lan, Y.; Keitz, B. K.; Liu, P.; Endo, K.; Day, M. W.; Houk, K. N.; Grubbs, R. H. *J. Am. Chem. Soc.* **2012**, *134*, 7861.
(13) For a recent view, see: Hartwig, J. *Inorg. Chem.* **2007**, *46*, 1936.
(14) For a recent review, see: Lu, X.-Y. *Top. Catal.* **2005**, *35*, 73.
(15) (a) Netherton, M. R.; Dai, C.-Y.; Neuschutz, K.; Fu, G. C. *J. Am. Chem. Soc.* **2001**, *123*, 10099. (b) Zhou, J.; Fu, G. C. *J. Am. Chem. Soc.* **2003**, *125*, 14726. (c) Han, C.; Buchwald, S. L. *J. Am. Chem. Soc.* **2009**, *131*, 7532. (d) Kambe, N.; Iwasaki, T.; Terao, J. *J. Chem. Soc. Rev.* **2011**, *40*, 4937.
(16) The buried volume of a ligand ($\%V_{bur}$) is defined as the percentage of volume occupied by the ligand in the first coordination sphere of the metal; see: (a) Hillier, A. C.; Sommer, W. J.; Yong, B. S.; Petersen, J. L.; Cavallo, L.; Nolan, S. P. *Organometallics* **2003**, *22*, 4322. (b) Dorta, R.; Stevens, E. D.; Scott, N. M.; Costabile, C.; Cavallo, L.; Hoff, C. D.; Nolan, S. P. *J. Am. Chem. Soc.* **2005**, *127*, 2485. (c) Cavallo, L.; Correa, A.; Costabile, C.; Jacobsen, H. *J. Organomet. Chem.* **2005**, *690*, 5407. (d) Poater, A.; Cavallo, L. *Dalton Trans.* **2009**, 8878. (e) Poater, A.; Cosenza, B.; Correa, A.; Giudice, S.; Ragone, F.; Scarano, V.; Cavallo, L. *Eur. J. Inorg. Chem.* **2009**, 1759. (f) Clavier, H.; Nolan, S. P. *Chem. Commun.* **2010**, *46*, 841. (g) Ragone, F.; Poater, A.; Cavallo, L. *J. Am. Chem. Soc.* **2010**, *132*, 4249.
(17) Liu, P.; Montgomery, J.; Houk, K. N. *J. Am. Chem. Soc.* **2011**, *133*, 6956.
(18) (a) Ragone, F.; Poater, A.; Cavallo, L. *J. Am. Chem. Soc.* **2010**, *132*, 4249. (b) Poater, A.; Ragone, F.; Mariz, R.; Dorta, R.; Cavallo, L. *Chem.—Eur. J.* **2010**, *16*, 14348. (c) Wucher, P.; Caporaso, L.; Roesle, P.; Ragone, F.; Cavallo, L.; Mecking, S.; Gottker-Schnetmann, I. *Proc. Natl. Acad. Sci. U.S.A.* **2011**, *108*, 8955.
(19) Frisch, M. J.; et al. *Gaussian 09, Rev. B.01*; Gaussian, Inc.: Wallingford, CT, 2010.
(20) For dispersion correction, see: (a) Grimme, S. *J. Comput. Chem.* **2006**, *27*, 1787. (b) Grimme, S.; Antony, J.; Ehrlich, S.; Krieg, H. *J. Chem. Phys.* **2010**, *132*, 154104. For examples of employing dispersion corrected DFT calculations: (c) Lonsdale, R.; Harvey, J. N.; Mulholland, A. J. *J. Phys. Chem. Lett.* **2010**, *1*, 3232. (d) McMullin, C. L.; Jover, J.; Harvey, J. N.; Fey, N. *Dalton Trans.* **2010**, *39*, 10833. (e) Comas-Vives, A.; Harvey, J. N. *Eur. J. Inorg. Chem.* **2011**, 5025. (f) Jacobsen, H.; Cavallo, L. *ChemPhysChem* **2012**, *13*, 562.
(21) Legault, C. Y. *CYLView, 1.0b*; Université de Sherbrooke, Canada, 2009; http://www.cylview.org.
(22) In the study of the mechanisms, 1,3-dimethylimidazolidine (SIMe) was used as a model ligand, which is represented by L in Figures 1, 3, and 5. The SIPr ligand was employed in test calculations for **TS11** and **TS19**. **TS11** is more than 20 kcal/mol more stable than **TS19** with the SIPr ligand, in agreement with calculations with the model ligand.
(23) For related discussions of the possible pathways: (a) Saito, N.; Tanaka, D.; Mori, M.; Sato, Y. *Chem. Rec.* **2011**, *11*, 186. (b) See ref 4f.
(24) Wang, S. C.; Troast, D. M.; Conda-Sheridan, M.; Zuo, G.; LaGarde, D.; Louie, J.; Tantillo, D. J. *J. Org. Chem.* **2009**, *74*, 7822.
(25) For related Ni-catalyzed cyclization of alkynes, see: (a) Kumar, P.; Prescher, S.; Louie, J. *Angew. Chem., Int. Ed.* **2011**, *50*, 10694. (b) Kumar, P.; Troast, D. M.; Cella, R.; Louie, J. *J. Am. Chem. Soc.* **2011**, *133*, 7719. (c) Stolley, R. M.; Maczka, M. T.; Louie, J. *Eur. J. Org. Chem.* **2011**, *20*, 3815. (d) Kumar, P.; Louie, J. *Org. Lett.* **2012**, *14*, 2026.
(26) Experimentally, the reaction is complete at room temperature within several hours, suggesting the overall barrier of reaction is around 20 kcal/mol.
(27) For recent examples of DFT studies, in which the steric effect of ligand or substrate is crucial for the selectivity, see: (a) Zhou, J.-L.; Liang, Y.; Deng, C.; Zhou, H.; Wang, Z.; Sun, X.-L.; Zheng, J.-C.; Yu, Z.-X.; Tang, Y. *Angew. Chem., Int. Ed.* **2011**, *50*, 7874. (b) Qu, J.-P.; Liang, Y.; Xu, H.; Sun, X.-L.; Yu, Z.-X.; Tang, Y. *Chem.—Eur. J.* **2012**, *18*, 2196. (c) Yu, H.-Z.; Jiang, Y.-Y.; Fu, Y.; Liu, L. *J. Am. Chem. Soc.* **2010**, *132*, 18078.